

Toward Tissue-Like Material Properties: Inducing In Situ Adaptive Behavior in Fibrous Hydrogels

Wen Chen, Jyoti Kumari, Hongbo Yuan, Fan Yang, and Paul H. J. Kouwer*

The materials properties of biological tissues are unique. Nature is able to spatially and temporally manipulate (mechanical) properties while maintaining responsiveness toward a variety of cues; all without majorly changing the material's composition. Artificial mimics, synthetic or biomaterial-based are far less advanced and poorly reproduce the natural cell microenvironment. A viable strategy to generate materials with advanced properties combines different materials into nanocomposites. This work describes nanocomposites of a synthetic fibrous hydrogel, based on polyisocyanide (PIC), that is noncovalently linked to a responsive cross-linker. The introduction of the cross-linker transforms the PIC gel from a static fibrous extracellular matrix mimic to a highly dynamic material that maintains biocompatibility, as demonstrated by in situ modification of the (non)linear mechanical properties and efficient self-healing properties. Key in the material design is cross-linking at the fibrillar level using nanoparticles, which, simultaneously may be used to introduce more advanced properties.

material chemists can only dream of realizing this level of adaptiveness. In search of artificial matrices that better mimic the cell's microenvironment, nature's fibrous hydrogels are arguably the best starting point. The fibrous architectures give rise to good mechanical properties at low protein densities and ensure a porous matrix that facilitates cell migration. A key hallmark of such matrices is strain stiffening, i.e., the effect that the stiffness of the hydrogel strongly (up to 100-fold) and reversibly increases as the material is deformed.^[2] Indeed, networks of extracellular matrix proteins collagen^[3] and fibrin^[4] but also cytoskeletal proteins actin^[5] and intermediate filaments^[6] all show a strain stiffening response which is crucial for the complex mechanical response of tissues.^[7] Depending on the protein, the threshold (sensitivity to deformation) and the extent of stiffening (responsiveness to deformation) varies.

Although (reconstituted) hydrogels of biopolymers recapitulate the architecture and mechanical properties of the ECM relatively well, they are difficult to tailor and manipulate. Oppositely, synthetic fibrous gels in combination with on-demand adaptivity would give rise to uniquely tailorable materials,^[8] which may be at the basis of the next generation of matrix materials for cell culture and tissue engineering.^[9]

These synthetic equivalent remain relatively rare. Our group reported an early example based on polyisocyanide (PIC) gels with a semiflexible bundled architecture that closely mimics intermediate filaments.^[10] Sijbesma and co-workers developed fibrous hydrogels from covalent fixed of bisurea bolamphiphiles^[11] and, recently, van Esch and co-workers reported a new class of self-assembling semiflexible fibrous gels.^[12] Beyond the approach of rigid components, also strain stiffening behavior of hybrid flexible gels^[13] and cleverly engineered materials^[14] have been reported. Although these materials reliably show strain stiffening behavior, to further manipulate the mechanical properties, researchers typically vary the polymer concentration, which, however changes all other hydrogel properties simultaneously. Strategies to fabricate hydrogels mimicking the dynamic properties and high adaptiveness of the native ECM are highly challenging.

An emerging strategy to design stimuli-responsive polymeric hydrogels employs composites or hybrids: polymer gels with nanoparticles that provide new physical, chemical, and biological properties.^[15] A well-designed interaction between polymer


1. Introduction

Living cells continuously probe the mechanical properties of their microenvironment, and simultaneously, generate physical feedback to remodel and reorganize the extracellular matrix (ECM) by protein excretion or digestion, which allows them to actively, in situ, manipulate the matrix mechanics.^[1] So far,

W. Chen, J. Kumari, F. Yang, P. H. J. Kouwer
Institute for Molecules and Materials
Radboud University
Heyendaalseweg 135, Nijmegen AJ 6525, The Netherlands
E-mail: p.kouwer@science.ru.nl

H. Yuan
Molecular Imaging and Photonics
Chemistry Department
KU Leuven
Celestijnenlaan 200F, Heverlee 3001, Belgium

H. Yuan
Institute of Biophysics
Hebei University of Technology
Tianjin 300401, P. R. China

 The ORCID identification number(s) for the author(s) of this article can be found under <https://doi.org/10.1002/adma.202202057>.

© 2022 The Authors. Advanced Materials published by Wiley-VCH GmbH. This is an open access article under the terms of the Creative Commons Attribution-NonCommercial License, which permits use, distribution and reproduction in any medium, provided the original work is properly cited and is not used for commercial purposes.

DOI: 10.1002/adma.202202057

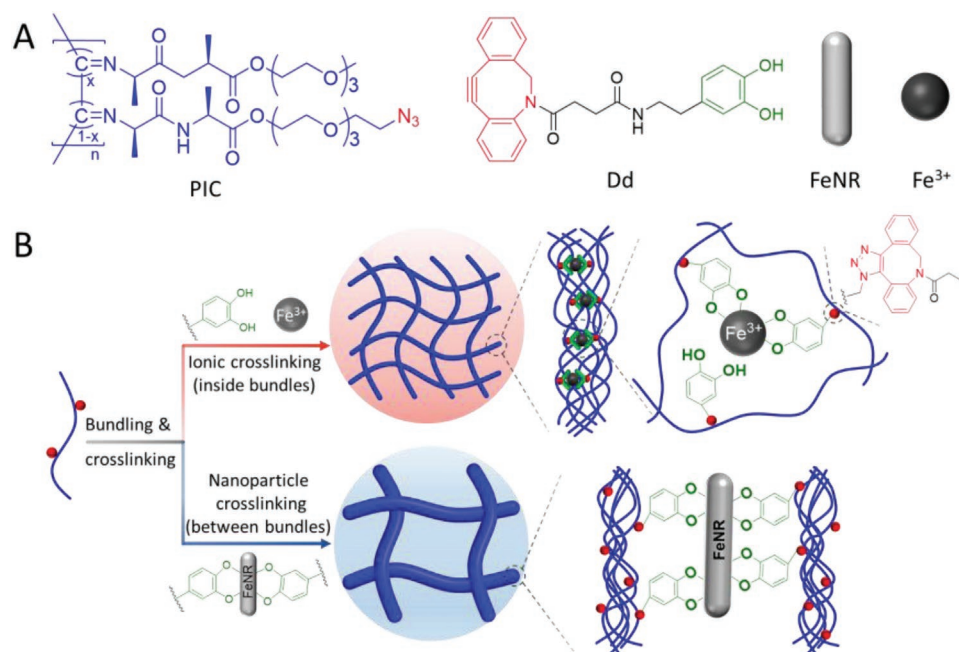


Figure 1. Materials and strategies used to develop the adaptive hydrogels. A) Molecular structure of the azide-functionalized polyisocyanide (PIC), the short spacer (Dd) with a dual purpose (in the ionic cross-linking approach and in the particle cross-linking approach as functional groups grafted on the FeNR surface). B) Chain bundling network formation attributed to hydrophobic interactions of the polyisocyanide backbone and the ethylene glycol tails. Ionic cross-linking via the SPAAC reaction and metal-coordination interactions in the mixture of PIC, Dd, and iron ions results in the inside bundling cross-linking process without changing the morphology of the gel network. Nanoparticle cross-linking in the mixture of PIC and Dd-functionalized FeNRs results in between bundling cross-linking with the formation of a polymer–particle network.

and nanoparticle (NP) (e.g., based on metal-coordination bonding,^[16] hydrogen bonding,^[15a] host–guest interactions,^[17] and dynamic covalent bonding^[18]) can be used to introduce unique behavior including sensitivity to external cues (magnetic, pH responsiveness, etc.), self-healing properties, anisotropy, conductivity, and so on. Inspired from marine mussel threads,^[19] catechol groups were found to efficiently form reversible hydrogen bonding^[15a,20] and metal–catechol coordination;^[21] and were used to develop hydrogels with self-healing properties, adhesiveness, and stimuli responsiveness.^[22]

Here, we describe a comprehensive strategy to dynamically manipulate the linear and nonlinear (strain stiffening) mechanics of biomimetic hydrogels. As the core material, we use the highly responsive PIC-based hydrogel (Figure 1A).^[2b,10] To induce dynamic properties in this static fibrous gel, we introduce responsive cross-linkers, either at the polymer chain level or at the mesh size level, following two distinctly different approaches (Figure 1B). In the first, which we term ionic cross-linking, we use ferric ions (Fe^{3+}) that primarily cross-link inside bundles of the PIC network. A maximum of three catechol ligands are able to bind to one cation. In the second strategy, termed nanoparticle cross-linking, iron oxide nanorods (FeNRs) act as cross-linkers, which allow many more bonds between the polymers and one particle. As the length of the FeNRs is of the order of the mesh size of the PIC network, one would expect that this strategy will also cross-link between different bundles. For the interaction between the polymer and the Fe^{3+} ions or the FeNRs, we employ a small spacer with, at one terminus, a dibenzocyclooctyne (DBCO) group that can covalently bind

to the azide groups on the PIC and on the other terminus a dopamine moiety that forms a dynamic metal-coordination bond to the ion or nanoparticle (Figure 1A).^[19] The dynamic character in the gel, which is the result of the noncovalent (pH sensitive) dopamine– Fe^{3+} /FeNP junctions, is best demonstrated by the excellent self-healing properties gel. In this paper, we provide tools to direct mechanical properties (linear and strain stiffening) and dynamics of these fibrous hydrogels, simply by controlling the nature of the cross-link, its density, and its affinity.

2. Results

2.1. Preparation of Hydrogel Composites

For the strain stiffening hydrogel, we employed the fully synthetic semiflexible ethylene-glycol-substituted PIC polymers.^[10] On heating an aqueous PIC solution above T_{gel} , the PIC chains aggregate into bundles and form a thermoresponsive hydrogel network,^[23] analogous to hydrogels of intermediate filaments or F-actin.^[2b,10] As such, PIC gels have been exploited as a biomimetic material for various biomedical applications that range from in vitro cell culture material^[24] (as an artificial ECM) to in vivo wound healing^[25] and dental^[26] applications. As a synthetic polymer, however, it provides excellent molecular control in physical and chemical properties. Functional groups at the periphery of the polymer chain (like the azide group) are readily postfunctionalized to virtually any moiety, including peptides,

proteins, and dyes.^[27] Their mechanical properties can be tailored by varying many (orthogonal) parameters, including the polymer concentration^[10] and length, and the application of external stimuli, like temperature,^[10,28] ionic strength of the solution,^[28a] cross-links,^[29] and external or internal mechanical forces.^[23,30]

For the cross-linking reactions, PIC was equipped with azide groups (10 mol%) following established protocols^[24b] (see the Supporting Information for details). Ferromagnetic FeNRs (Fe₃O₄) were synthesized earlier^[31] and functionalized with different densities of dopamine–DBCO (dD) linkers at their surfaces (Supporting Information). For the FeNP cross-linking procedure, a cold PIC solution (4 °C) was mixed with a cold solution (4 °C) of the dD-functionalized FeNRs. After mixing, the solution is heated to 37 or 50 °C to accelerate the strain-promoted azide–alkyne cycloaddition (SPAAC) cross-linking reaction, which was considered finished when the mechanical properties of the nanocomposite stabilized. Note that higher cross-linking temperatures require shorter reaction times.^[31] For the ionic cross-linking, a cold solution of PIC and a solution with the required concentration of dD linkers and a fixed concentration (excess) of FeCl₃ were mixed and heated to 37 °C for the SPAAC reaction to complete. The reaction with these dynamic cross-linkers are much faster than those with the FeNPs.^[32]

For rheology experiments, the SPAAC reaction is performed in situ in between the parallel plates of the rheometer. After cross-linking, the temperature is lowered to 5 °C, where uncross-linked PIC returns to an aqueous solution, while for the cross-linked samples, the gel state is (partly) maintained. We then heat all samples to 37 °C where the nonlinear strain stiffening properties of the materials are assessed via the prestress protocol,^[2b,33] which accurately captures the mechanical properties of a material under strain by superposing a small oscillatory stress on a larger constant stress σ . From the protocol, we calculate the differential modulus $K' = \delta\sigma/\delta\gamma$, where $\delta\sigma$ and $\delta\gamma$ represent the oscillatory stress and strain, respectively. At low applied (pre)stress, i.e., in the linear viscoelastic regime, K' equals the common shear modulus G' but beyond a critical stress σ_c , which marks the stress onset for nonlinearity, a strong stiffening regime is entered and the modulus increases exponentially with applied stress following $K' \propto \sigma^m$. The stiffening index m , with the theoretical limit^[34] $m \leq 3/2$, determines the intensity of the stiffening response.

2.2. The Effect of the Cross-Linker on the Linear and Nonlinear Mechanical Properties

Variation of the mechanical properties of fibrous hydrogels typically addresses through the protein concentration, which has the disadvantage that many other properties vary simultaneously. In vivo and in vitro, however, cross-linking is used as an effective strategy. In our PIC model, we studied two cross-linking extreme systems' cross-linking modes: the first where the cross-links are positioned inside the fibrils; the second where they are between fibrils, both using the same noncovalent iron coordination motif. We anticipate that the intrafibrillar cross-links will not significantly change the fibrous architecture and, based on earlier work,^[29] will not change the linear

and nonlinear mechanical properties of the gels significantly. Contrarily, cross-links between bundles will affect the network architecture and for these gels,^[31] we would expect a strong dependence on the degree of connectivity between the polymer network and the nanoparticles.

We prepared cross-linked gels with a fixed polymer concentration, [PIC] = 1 mg mL⁻¹, corresponding to 350 μ m available azide groups). For the intrafibrillar-cross-linked hydrogels, denoted PIC^{Fe3+}, excess iron Fe³⁺ (667 mM) was introduced and the concentration of the linker was varied to give samples PIC^{Fe3+}-1 to PIC^{Fe3+}-4 (Table 1). The nanoparticle-conjugated gels, denoted PIC^{FeNR} are prepared with a fixed nanoparticle concentration [FeNRs] = 1 mg mL⁻¹. As controls, we included pure PIC gels (without Fe³⁺ or nanorods) and the corresponding physical mixture at the same PIC and FeNR concentration but without linkers. After mixing, the samples were heated for cross-linking, cooled to 5 °C, and reheated to 37 °C (Figure S2 in the Supporting Information for the full experiment).

As the PIC gels are thermoreversible, cooling a gel that has not been cross-linked yields the polymer solution, whereas cross-linked gels (partially) maintain their stiffness. From the reheating curve, we determine a phenomenological cross-linking efficiency S as the ratio of the shear modulus at $T = 5$ and 37 °C: $S = G'_{5^\circ\text{C}}/G'_{37^\circ\text{C}}$, which assumes that for a highly cross-linked PIC hydrogel, the thermoreversibility is entirely suppressed. In addition, we define a cross-linking-induced stiffening ratio R , which is the ratio between the shear modulus of the cross-linked sample with that of the PIC gel, both at 37 °C: $R = G'_{37^\circ\text{C}}/G'_{\text{PIC}}$.

Figure 2A and Table 1 summarize the mechanical properties of all composites and the controls in the linear viscoelastic regime (LVE). The curves of ionically cross-linked Fe³⁺ gels (open squares) virtually overlap; a small increase in stiffness

Table 1. Mechanical properties of the cross-linked composites. For all samples: [PIC] = 1 mg mL⁻¹ and [Fe³⁺] = 350 μ M or [FeNR] = 1 mg mL⁻¹. Mechanical properties as the average of 3 measurements with the standard deviation.

Gel	Linker concentration [μ M]	$G'_{5^\circ\text{C}}$ [Pa]	$G'_{37^\circ\text{C}}$ [Pa]	Cross-linking efficiency S^a	Stiffening ratio R^b
PIC only ^c	–	0.58 \pm 0.06	118 \pm 22	–	1
PIC ^{Fe3+} -1	175	12 \pm 3	82 \pm 12	0.15	0.69
PIC ^{Fe3+} -2	350	16 \pm 4	88 \pm 15	0.18	0.75
PIC ^{Fe3+} -3	525	28 \pm 9	110 \pm 48	0.25	0.93
PIC ^{Fe3+} -4	700	40 \pm 7	119 \pm 35	0.33	1.01
PIC ^{FeNP} -1	122	10 \pm 1	127 \pm 31	0.08	1.1
PIC ^{FeNP} -2	186	38 \pm 8	157 \pm 20	0.24	1.3
PIC ^{FeNP} -3	265	81 \pm 1	223 \pm 36	0.36	1.9
PIC ^{FeNP} -4	372	142 \pm 32	227 \pm 36	0.63	1.9
PIC ^{FeNP} -5	562	311 \pm 99	379 \pm 60	0.82	3.2
PIC ^{FeNP} -6	850	1003 \pm 167	892 \pm 110	1.12	7.6
PIC + FeNRs ^d	–	0.43 \pm 0.02	93 \pm 20	–	0.8

^a)Cross-linking efficiency $S \equiv G'_{5^\circ\text{C}}/G'_{37^\circ\text{C}}$; ^b)Stiffening ratio $R \equiv G'_{37^\circ\text{C}}/G'_{\text{PIC}}$; ^c)Control 1: PIC gel only; no Fe³⁺, FeNPs, or linkers added; ^d)Control 2: physical mixture of PIC and FeNR without linkers.

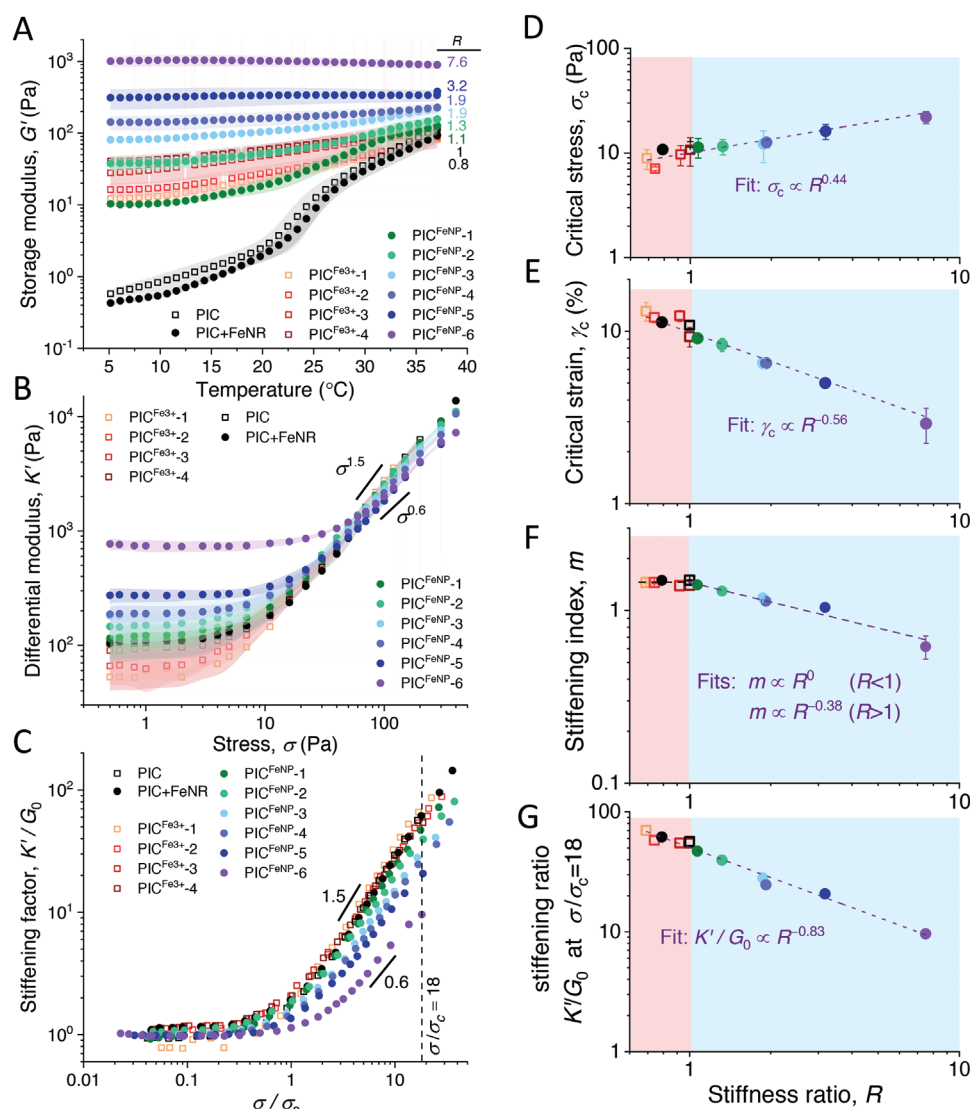


Figure 2. Mechanical properties of the cross-linked composite gels as a function of the cross-link density. A) Shear modulus G' in the LVE as a function of temperature T measured for samples with different cross-linking efficiency, obtained in the reheating curves. B) Strain stiffening data: differential modulus K' as a function of applied stress σ for the same samples, showing little variation for the Fe^{3+} -cross-linked gels and a decrease from $K' \propto \sigma^{1.5}$ to $K' \propto \sigma^{0.6}$ at high FeNP cross-linking densities. C) K' versus σ with the modulus and stress normalized with G_0 and σ_c , respectively, clearly showing the reduced stiffening response for the FeNP-cross-linked gels. D–G) Data extraction from the nonlinear measurements: critical stress σ_c (D), critical strain $\gamma_c = \sigma_c/G'$ (E), stiffening index m (F), and stiffening factor K'/G_0 (G) plotted against the stiffening ratio R . Data are averages of $n = 2–4$ experiments; shading in (A–C) or error bars in (D–G) represent standard deviation. The solid lines in (D–G) are power-law fits. For all samples: $[\text{PIC}] = 1 \text{ mg mL}^{-1}$, $[\text{Fe}^{3+}] = 667 \text{ }\mu\text{M}$ or $[\text{FeNRs}] = 1 \text{ mg mL}^{-1}$, only the molar ratio of linkers varies.

is observed for higher linker densities. The storage moduli at $T = 37 \text{ }^\circ\text{C}$ are in line with that of the PIC gel (black squares), indicating that, indeed, the ions hardly interfere with the network architecture and mainly stabilize the existing fibrillar structure, which become clear on cooling: at low temperatures, the PIC gel transforms to a solution, while the ferric ions stabilize the polymer chain in the bundles, which (partly) maintains the network. Note that none of the samples show signs of relaxation in the frequency range 0.1–10 Hz (Figure S3A,B, Supporting Information).

The mechanical properties of the nanorod-cross-linked hydrogels (solid circles) strongly depend on the connectivity between

the network and the particles. First, with an increasing density of linkers on the nanorods, the thermoreversibility of the PIC gradually disappears completely; at the highest cross-linking densities, the shear modulus has become nearly independent of temperature (Figure S3C,D in the Supporting Information for viscoelasticity). In contrast to the ferric ions, the nanorod-based cross-linking strongly affects the shear modulus in the gel phase: $G'_{37^\circ\text{C}}$ increases to $\approx 1000 \text{ Pa}$ for the strongest cross-linked composite, corresponding to $R = 76$. The stiffening effect is attributed^[31] to a change in morphology of the network induced by the cross-linking reaction, where the bundle thickness increases from 11 to 300 nm (Figure S4, Supporting Information).

In the nonlinear stiffening regime, we find that ionic cross-linking (Figure 2B) has a negligible effect on the stiffening response; irrespective of the number of cross-links, the samples behave the same as the PIC only control, which become particularly clear when the data are normalized to G' and σ_c (Figure 2C). Analogous to the LVE regime, nanoparticle cross-linking has a clear effect on strain stiffening of the composites. Increasing the interaction between the particles and the polymer network increases σ_c and decreases m . In other words, the composites become less sensitive and less responsive toward external strain with an increasing degree of cross-linking. The stiffening index, m , decreases from 1.5 for pure PIC (also found for gels of intermediate filaments and actin) to 0.6 (close to values found for fibrin gels) for the composite with highest cross-linking efficiency.^[2a] Normalization to G' and σ_c clearly shows that the stiffening of different gels does not collapse to a single master curve, which is often observed in concentration or temperature studies.^[2b,28a] We note that these results were not predicted by modeling studies of cross-linked idealized semiflexible networks.^[35] In fact, our data indicate that with the same composition, a high variability of mechanical properties can be realized. Earlier work that aimed to tune the strain stiffening parameters, always require compositional changes or variation in the experimental conditions. More commonly, cross-linking of networks based on, for example, actin,^[5] proteins,^[36] modular gelators,^[12] and micelles,^[11] show unchanged stiffening responses.

When we consider that the increase in stiffness, as quantified by R , originates from a morphological change in the network that is induced by the cross-linking reaction, we may expect that the nonlinear mechanical parameters will also scale to R .^[24b] Interestingly, we observe that all parameters show a power law relation with R over the experimentally accessible regime (Figure 2D–G). The critical stress σ_c scales with $R^{0.44}$ and the critical strain $\gamma_c = \sigma_c/G_0 \sim R^{-0.56}$. The latter shows that the tighter cross-linked gels become more sensitive to small deformations, something that is usually not observed in concentration variations^[2b] but may have important consequences for in vitro or other soft matter applications. Also, the stiffening factor K'/G_0 determined at a set relative stress $\sigma/\sigma_c = 18$ and the stiffening index m scales directly to R and, thus, to the thickening of the bundles inside the composite. In short, the ionic cross-linking has a negligible effect on the linear and nonlinear mechanics of the polymer network itself; while the mechanics of the polymer–particle network strongly depend on the connectivity between the two components. Increasing the connectivity increases the gel stiffness in the LVE regime and decreases the stiffening response in the high stress regime.

To our best knowledge, this is the first example where the nonlinear strain stiffening parameters are so extensively tailored without changing the concentration of the components. The “between-bundles” cross-linking approach proves a relatively easy but highly effective way to control hydrogel mechanics. The approach is analogous to the cell, where cross-linking of the different cytoskeletal components is used to drive the mechanical properties.^[37] In synthetic systems, however, the linker density is not always readily adjusted, particu-

larly in 3D samples, and one should consider using stimuli-responsive cross-linkers to design tunable strain stiffening gels in situ. Since our cross-linking strategy is based on a metal-coordination interaction, we study in the next section how to exploit this interaction to manipulate the cross-link density in situ and, simultaneously, the linear and nonlinear mechanical parameters.

2.3. pH-Responsive Mechanics

Previous work showed that in gels of catechol-functionalized polymers cross-linked with ferric ions, a pH change influences the coordination of the ion to form mono, bis, or tris-dentate catechol complexes,^[38] which directly affect the mechanical properties of the gels. In our work, we hypothesize that, analogously, the pH will affect the coordination of the catechol to the Fe^{3+} ions (Figure 3A) or FeNRs (Figure 3B). Following our results from the previous section, we expect a minimal pH-dependence of the linear and nonlinear PIC^{Fe3+} gel mechanics, but a much stronger dependence on the mechanical properties of the PIC^{FeNP} gels.

To study the effect of pH on the intrafibrillar-cross-linked hydrogels, we used PIC^{Fe3+}-2 with intermediate cross-link density, i.e., with a 1:1 molar ratio of azide groups on the polymer and linker (Table 2). Note that the values at pH = 7 in buffer differ slightly from the results in MilliQ.^[39] For the pH range 6–9, the mechanical properties in the gel phase ($T = 37^\circ\text{C}$) are comparable to the PIC control at pH = 7 (the PIC controls are not sensitive to a change in pH; data are given in Figures S5A and S6A and Table S2 in the Supporting Information). We only find that the pH influences the stiffness at 5°C , resulting in an increasing cross-linking efficiency S at high pH (Figure S6B,C in the Supporting Information with frequency data). This result was expected as, in this case, the cross-links do not affect the network architecture, nor the mechanical properties. Only at low temperatures, we observe at lower pH a higher stability of the gels, i.e., a higher stability for materials that have more catechol groups bound to a single Fe^{3+} ion.

For the nanoparticle-cross-linked gels, a much stronger dependency on pH is observed. In these materials, also in the gel phase, the mechanical properties depend on the connectivity between polymer chains and particles, which, in turn depends on the pH of the solution. We studied the intermediately cross-linked gel PIC^{FeNP}-4 (cross-linking efficiency $S \approx 0.5$ at pH 7) and find that all samples are cross-linked to some degree; none of the gels completely collapse at 5°C (Figure S6D,E in the Supporting Information for frequency data). At pH 9, a cross-linked composite hydrogel with $S = 0.92$ (nearly fully cross-linked) and $R = 4.5$ is formed (Table 2 and Figure 3C). These values are comparable to PIC-^{FeNP} gels with a much higher cross-linker density (Figure 2A). The clearest indication of the different degree of cross-linking with pH is the shear modulus at $T = 5^\circ\text{C}$ which ranges from 16 Pa at pH 5 to 480 Pa at pH 9.

Fully in line with the linker density study, we observe that in the high stress regime (Figure 3D), the ferric-ion-cross-linked gels (square symbols) behave similar to the PIC controls (black symbols, Figure S5B,C, Supporting Information) and that the nonlinear mechanical properties of the

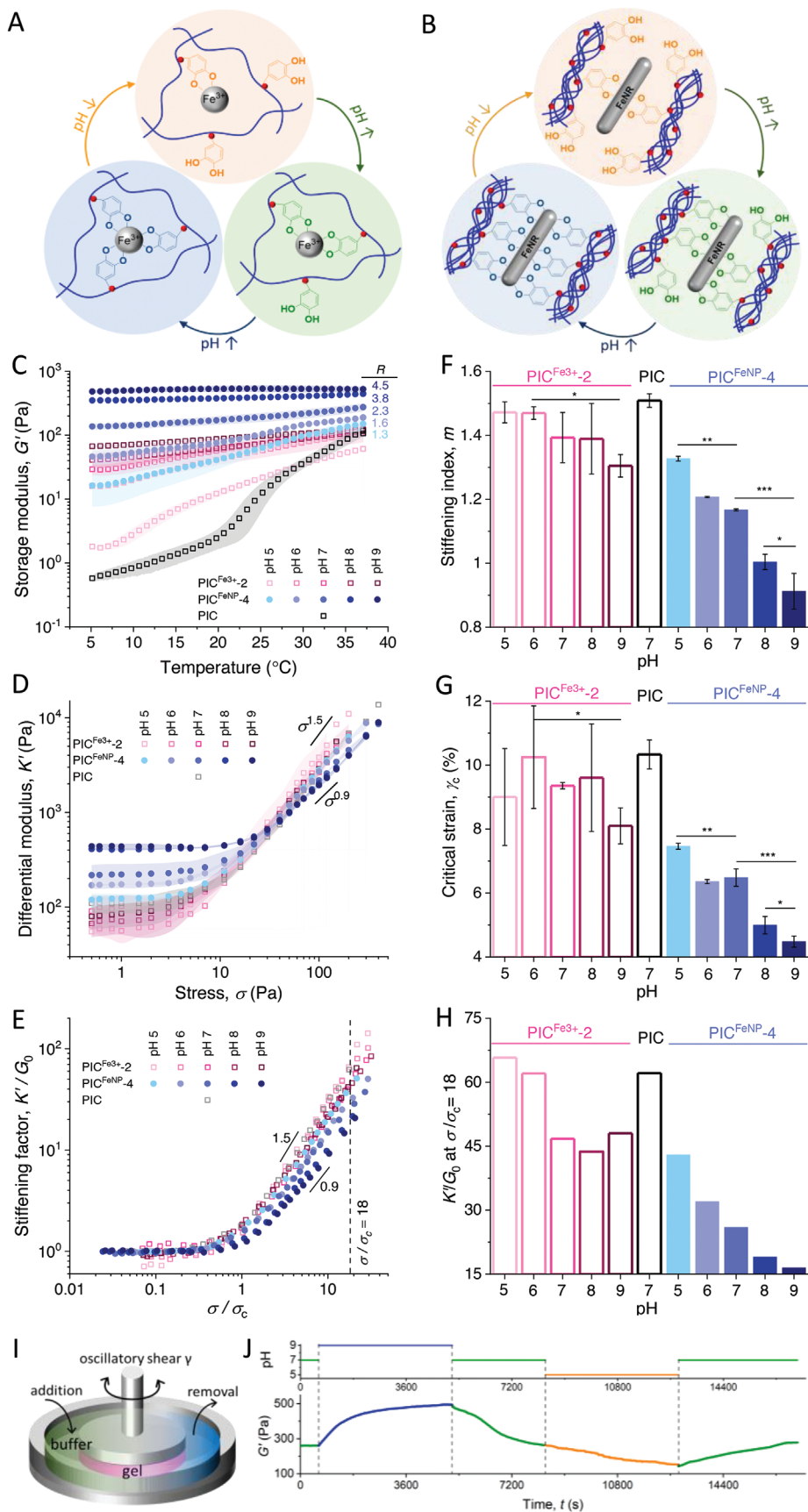


Table 2. Mechanical properties of the cross-linked composites at different pH. For all samples: [PIC] = 1 mg mL⁻¹ and [Fe³⁺] = 350 μM or [FeNR] = 1 mg mL⁻¹. Mechanical properties as the average of 3 measurements with the standard deviation.

Gel	pH	Linker concentration [μM]	$G'_{5^\circ\text{C}}$ [Pa]	$G'_{37^\circ\text{C}}$ [Pa]	Cross-linking efficiency S^a	Stiffening ratio R^b
PIC only ^{c)}	7	–	0.6 ± 0.1	117 ± 22	–	1
PIC ^{Fe3+} -2	5	350	1.8 ± 0.02	61 ± 1	0.03	0.52
PIC ^{Fe3+} -2	6	350	16 ± 0.2	111 ± 33	0.14	0.94
PIC ^{Fe3+} -2	7	350	29 ± 5	124 ± 30	0.23	1.05
PIC ^{Fe3+} -2	8	350	41 ± 9	117 ± 4	0.35	0.99
PIC ^{Fe3+} -2	9	350	67 ± 2	123 ± 2	0.54	1.04
PIC ^{FeNP} -4	5	372	16 ± 9	151 ± 34	0.11	1.3
PIC ^{FeNP} -4	6	372	46 ± 11	190 ± 5	0.24	1.6
PIC ^{FeNP} -4	7	372	137 ± 14	275 ± 40	0.50	2.3
PIC ^{FeNP} -4	8	372	350 ± 0.1	445 ± 6	0.79	3.8
PIC ^{FeNP} -4	9	372	483 ± 27	525 ± 51	0.92	4.5

^{a)}Cross-linking efficiency $S \equiv G'_{5^\circ\text{C}}/G'_{37^\circ\text{C}}$; ^{b)}Stiffening ratio $R \equiv C'_{37^\circ\text{C}}/C'_{\text{PIC}}$; ^{c)}Control: PIC gel only; no Fe³⁺, FeNPs, or linkers added PIC at other pH values in Table S2 (Supporting Information).

nanoparticle-cross-linked gels (filled circles) strongly scale with pH. When K' is rescaled with G_0 and σ with σ_c , the curves do not collapse on to a single master curve, but rather show the deviation that corresponds to a difference in stiffening index values (Figure 3E and Figure S7 (Supporting Information)); more cross-linked materials become less responsive toward mechanical deformation. From all curves, the nonlinear stiffening parameters m , γ_c and stiffening factor K'/G_0 were extracted (Figure 3F–H). At the highest cross-link efficiency (pH = 9), the stiffening index of the PIC^{FeNP}-4 gel reduced to $m = 0.9$ (Figure 3F). As a result, we find that the extent of stiffening, reflected by K'/G_0 , in these cross-linked gels significantly reduces from 39 at pH = 5 to 17 at pH = 9 (Figure 3H), which are much lower than the PIC control or the compared to a value of 62–67 for the PIC gel control (Table S2, Supporting Information) or the PIC^{Fe3+} gels. In addition, we observe that γ_c of the PIC gel control is not affected by the pH (γ_c of the PIC^{Fe3+} also

shows small variations), while γ_c of PIC^{FeNP} gels decreases with increasing pH (Figure 3G), analogous to earlier observations. The latter result illustrates that the FeNP composites in a basic environment are much more sensitive toward relatively small deformations. In summary, by simply modifying the pH, we are able to tailor the linear and nonlinear mechanical properties of the polymer–particle network. The results highlight that the position, dimensions, and functionality of the cross-links are crucial to the mechanical response of the hydrogel.

As the catechol–iron bond is dynamic in nature, we expect that pH-controlled mechanical properties of the PIC^{FeNP} gels are not constant and can be modified in situ. To study this effect, we performed a rheology experiment, using a home-built cup-shaped bottom plate, wherein a desired buffer can be placed after the gel is formed, which then diffuses into the hydrogel (Figure 3I). A sample (PIC^{FeNP}-4) was loaded at the center of the bottom and after the top plate was lowered to the gap size (500 μm), the sample was heated from 5 to 37 °C. After stabilization for 5 min, 3 mL of MilliQ was added and the instrument cover was placed to avoid water evaporation. After cross-linking for 24 h, the excess MilliQ was carefully removed and replaced by a buffer solution to provide different pH environments (Figure 3I). Going from pH 7 to 9, the gel's stiffness roughly doubled (Figure 3J). Subsequent changes to the pH clearly demonstrate the dynamic and reversible variability of the mechanical properties of these composite gels. The dynamic pH responsiveness was also observed in the Fe³⁺-cross-linked gels (Figure S9, Supporting Information). We note that some (pH independent) hydrogel stabilization from hydrogen-bonding catechol groups is left in the absence of ferric ions (Figure S9C, Supporting Information).

Overall, the mechanical properties of the PIC gel itself is independent of pH. Cross-linking the hydrogel with pH-responsive elements can be used to tailor the mechanics by pH, in particular when the cross-links are placed between the fibers of the gels. Interestingly, the mechanical parameters that we retrieved from our pH study consistently and quantitatively scale to R , similarly as they did for the linker density study (Figure S8, Supporting Information). This result confirms that the mechanical properties are dominated by connectivity in the polymer–particle network and the resulting network morphologies. Modification of this architecture, in our case by pH modulation, is an attractive strategy to manipulate the mechanics of (strain stiffening) materials.

Figure 3. Mechanical properties of gels at different pH using ionic cross-linking and nanoparticle cross-linking approaches. A,B) Schematic overview of the effects of pH in Fe³⁺- (A) and FeNP- (B) cross-linked gels. C) Shear modulus G' as a function of temperature T of PIC^{Fe3+}-2 gels (open squares), PIC^{FeNP}-4 gels (filled circles), PIC (black) at different pH. D,E) Differential modulus K' as a function of applied stress σ of the same gels (D), rescaled with G_0 and σ_c to emphasize the different responses to shear stress. F–H) Stiffening parameters: stiffening index m (F), critical strain γ_c (G), and stiffening factor K'/G_0 at $\sigma/\sigma_c = 18$ (H) as determined from the rheology curves as a function of the pH for PIC^{Fe3+}-2 gels (open), PIC^{FeNP}-4 (filled), and PIC (black). Overall, the parameters show small variations for the Fe³⁺-cross-linked gels and for the FeNP-cross-linked gel, a strong decrease in m , γ_c , and K'/G_0 with increasing pH, showing that pH change is a very powerful strategy to also affect the nonlinear mechanical properties of these gels. Data are averages of $n = 2$ –4 experiments; shading in (A–C) or error bars in (D–G) represent standard deviation. Significance was determined through a paired t -test. Significant differences: *, $p \leq 0.05$; **, $p \leq 0.01$; ***, $p \leq 0.001$. I) Schematic overview of the rheology setup for in situ dynamic experiments. The hydrogel (pink) is formed between the plates in a larger cup. The cup allows for replacement of the aqueous phase with buffer solutions of different pH (green and blue) during the rheology experiment. J) G' of PIC^{FeNP}-4 as a function of time, showing a dynamic pH responsiveness. Experiment: gel was prepared and cross-linked at pH = 7, cooled, returned to 37 °C, and equilibrated for 10 min; pH 9 buffer was placed in the cup and G' is monitored while the pH of the gel slowly increases through diffusion. After 75 min, the pH 9 buffer was replaced by a pH 7 buffer, 55 min later by a pH 5 buffer, and later again by a pH 7 buffer, showing good reversibility of the mechanical properties. Conditions for all panels: For PIC^{Fe3+}-2 gels: [PIC] = 1 mg mL⁻¹, [linker] = 350 μM, and [Fe³⁺] = 667 μM; for PIC^{FeNP}-4 gels, [PIC] = 1 mg mL⁻¹, [linker] = 372 μM, and [FeNR] = 1 mg mL⁻¹. $T = 37$ °C (D–H, J).

2.4. Self-Healing Behavior of Fibrous Hydrogels

The dynamics of metal-coordination interactions have already been exploited to develop self-healing hydrogels.^[16,21a] Analogously, we anticipate that the dynamic interactions in the PIC composites may give rise to self-healing behavior. To this end, both composite systems, PIC^{Fe3+} and PIC^{FeNP}, as well as the PIC control were studied. We stress that the combination of the strain stiffening and self-healing properties is very unusual^[13a,c] and has never been reported for biological or biomimetic fibrous hydrogels.

All samples were prepared at pH = 9 in order to optimally benefit from the metal-coordination interactions. After the standard preparation procedure in the rheometer, the samples were subjected to repeating cycles of low ($\gamma = 1\%$) and high ($\gamma = 300\%$) strain. Typical crossover strains where $G' < G''$ are around 100% for all samples (Figure S10, Supporting Information). Preliminary studies that varied the polymer concentration indicated that efficient self-healing properties were found at relatively high PIC concentrations and intermediate cross-linker and linker concentrations (Figure S11, Supporting Information).

In a qualitative experiment, pure PIC, PIC^{Fe3+}, and PIC^{FeNP} hydrogels were generated on a Petri dish, cut in two pieces, and reconstituted by placing the cut interfaces together (Figure 4A–C). The pure PIC gel failed to join (Figure 4A and Video S1 (Supporting Information)), while the ionic- and nanoparticle-cross-linked gels healed at the interface and the gels maintained shape integrity under shaking (Figure 4B,C and Videos S2 and S3 (Supporting Information)).

More quantitative studies were carried out with the composites PIC^{Fe3+}-2 and PIC^{FeNP}-4 with a PIC concentration of 6 mg mL⁻¹ (dD linker concentrations of 2.1 and 1.45 mM, cross-linker concentration of [Fe³⁺] = 1 mM or [FeNPs] = 4 mg mL⁻¹, respectively). At these PIC concentrations, the stiffnesses of the ionic- and FeNP-cross-linked gels increase to 2 and 5 kPa, respectively; the PIC gel forms a gel with $G' = 1$ kPa (Figure 4D–F). When applying a 300% strain, all materials exhibited fluid-like, viscous behavior indicated by the pronounced decrease in G' . After cessation of the high strain, the recovery was monitored at 1% strain and 1 Hz frequency. PIC^{FeNP}-4 gels showed excellent mechanical recovery within seconds, even after 12 cycles (Figure 4F). Contrasting the quick and qualitative cutting experiment, only 10% of the original modulus retrieved after the first cycle of the corresponding ferric-ion-cross-linked gel, which decreased to 5% after 12 cycles (Figure 4E). As expected, the pure PIC showed minimal healing efficiency (Figure 4D).

The results indicate that the cross-linking mode is critical to the self-healing behavior. In the absence of cross-linker or when the cross-linker is situated between the polymer chains in the bundle, the hydrogel is unable to recover from a large deformation. In the plain PIC gel, the interactions between the polymer chains in the fibrils have been broken upon the large deformation and the gel character of the material largely disappeared (Figure 4G). We anticipate that for the ferric-ion-cross-linked gel, the interactions within the bundles, between the polymer chains fully recover. These interactions, however,

poorly contribute to the mechanical stability of the network at a larger scale after a large deformation disrupted the fibrillar network architecture, but are sufficient to provide local healing after a cut. Contrastingly, the nanoparticles form bonds between different fibrils and when they reform after the high strain is removed, they directly contribute to network integrity, provided that their number of interactions is sufficiently high. The experiments at lower PIC and FeNP concentrations ([PIC] = 1 or 3 mg mL⁻¹ and [FeNP] = 1 or 4 mg mL⁻¹, Figure S11, Supporting Information) show that a reduced density of interactions gives less efficient healing.

2.5. Biocompatibility of the Composites

To be able to apply such material in in vitro cell culture, basic biocompatibility must be established, which was studied using human foreskin fibroblasts (HFFs). The fibroblast were encapsulated in the 3D hydrogel composites, either containing ionic-cross-linked gels with low and highly cross-linking densities, or nanoparticle-cross-linked gels with low and high cross-linking densities. As controls the PIC gel alone and PIC–nanoparticle physical mixture were used. To allow cell–matrix interaction, we used for the cell work PIC polymers that were decorated with the cell-adhesive peptide Gly–Arg–Gly–Asp–Ser (GRGDS), analogous to earlier studies.^[24e] Note that the peptide conjugation uses the same, but with extra available azide groups on the polymer chain for cross-linking. The biocompatibility of the PIC gel has been well-established,^[24] also for HFFs.^[24e] Biocompatibility was studied with a live–dead assay, a proliferation assay based on mitochondrial activity, and a Comet assay to screen for DNA damage from the nanoparticles.

The live–dead images (Figure 5A) show viability in the different PIC gel culture systems, where calcein-AM (green) stains alive cells and TOTO-3 (red) stains dead cells. Image quantification yields viability values between 98% (for the PIC gels cross-linked with Fe³⁺) and 84% for the PIC/FeNP physical mixture and the densely cross-linked PIC^{FeNP}-6. Overall at day 5, viability is high to very high for all samples, which confirms that these matrices may be explored further for any other biological applications. Further, the bright field images (Figure 5B) showed excellent cell spreading as well as cell–cell attachment. Moreover, the black color of FeNR was also visible. We emphasize that PIC matrices are intrinsically not biodegradable and cannot be enzymatically remodeled. Cell migration is supported by physical remodeling mechanisms, as was earlier also found in nondegradable alginate gels.^[40]

Proliferation (Figure 5D) was measured at day 1 (striped columns) and day 5 (open/filled columns) through analysis of cellular mitochondrial activity through a commercially available Cell Counting Kit-8 (CCK8) assay. The results are represented as the absorbance at days 1 and 5. Fibroblast proliferation in the control and the FeNP mixture was in line with earlier studies,^[24e] however, the fold change from day 1 to day 5 for the nanoparticle-cross-linked gels was particularly high: 11.3 and 3.1 for PIC^{FeNP}-1 and PIC^{FeNP}-6, respectively. Overall, we conclude that for all conditions, proliferation is increasing

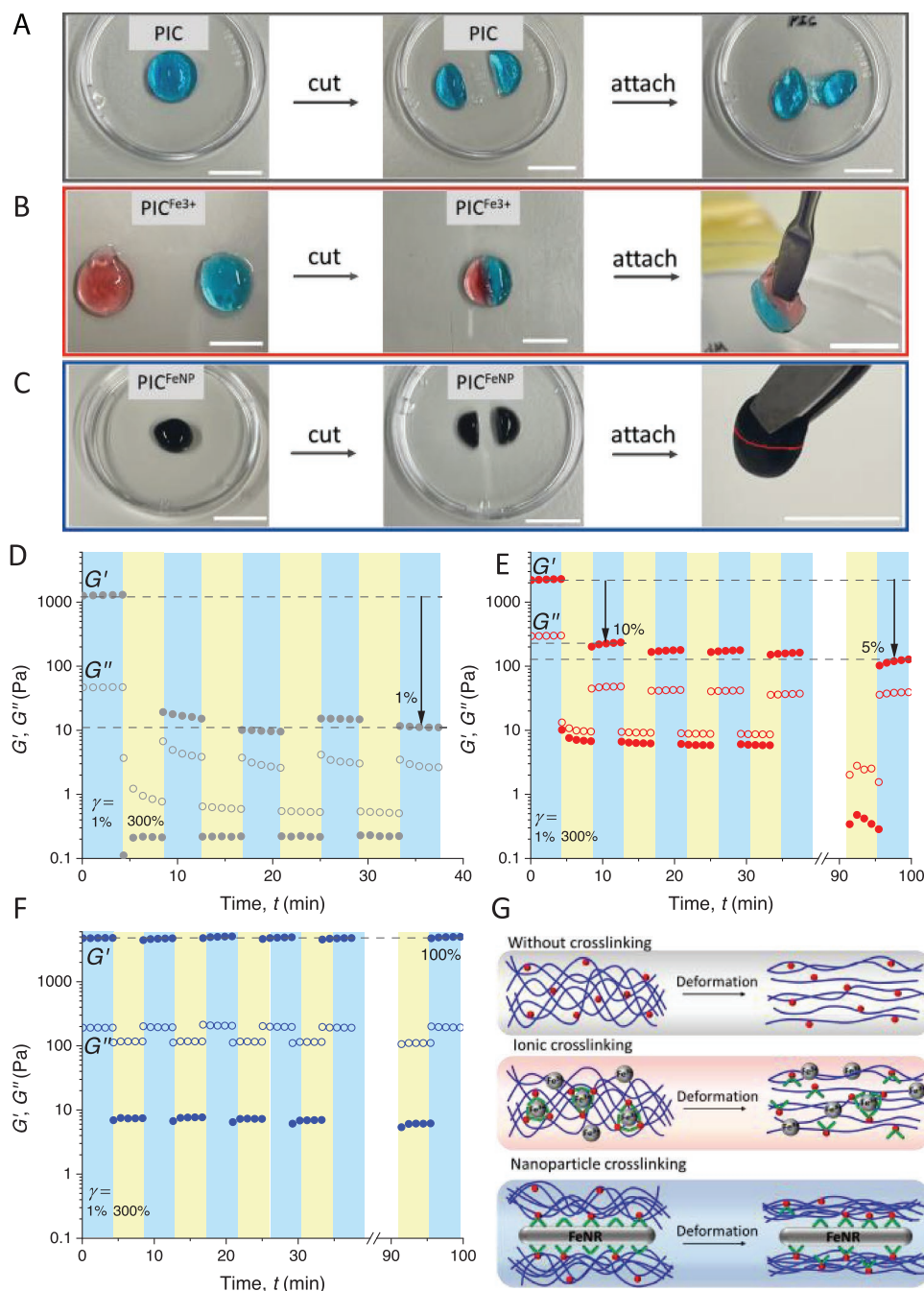


Figure 4. Self-healing properties of differently cross-linked PIC gels. A–C) Photos of the self-healing properties of PIC (A), ionic-cross-linked gels (B), and nanoparticle-cross-linked gels (C). The red line in (C) indicates the fractured interface. Movies of the experiment are available in the Supporting Information. D–F) Strain amplitude measurements at with strains cycling between 1% (blue background) and 300% (yellow) strain of PIC gels (no cross-linking) (D), ionic-cross-linked gels (E), and nanoparticle-cross-linked gels (F). Conditions: PIC control: [PIC] = 6 mg mL⁻¹; PIC^{Fe³⁺}-2 gel: [PIC] = 6 mg mL⁻¹, [linker] = 2100 μM, and [Fe³⁺] = 1000 μM; for PIC^{FeNP}-4 gels, [PIC] = 6 mg mL⁻¹, [linker] = 1448 μM, and [FeNP] = 4 mg mL⁻¹; all samples: T = 37 °C. Note, the linker/PIC ratio is the same as in the PIC^{Fe³⁺}-2 gel, ferric ions are in excess, and that FeNP concentration matches the PIC^{FeNP}-4 gel. G) Schematic illustration of the healing concept for the dynamic metal-coordination interactions in the different hydrogels.

in time, which further confirms biocompatibility of all (composite) hydrogels.

The Comet assay of cells treated with a high concentration of iron nanorods in the medium showed increased DNA damage as compared to control cells (Figure S12, Supporting Information),

which was in line with the results of previous studies.^[41] The tail moment of DNA was found to depend on nanoparticle concentration; a higher tail moment was visible in case of nanoparticle concentration of 1 mg mL⁻¹ (3.0 μm) compared to nanoparticle concentration of 10 μg mL⁻¹ (0.8 μm) and control (0.4 μm).

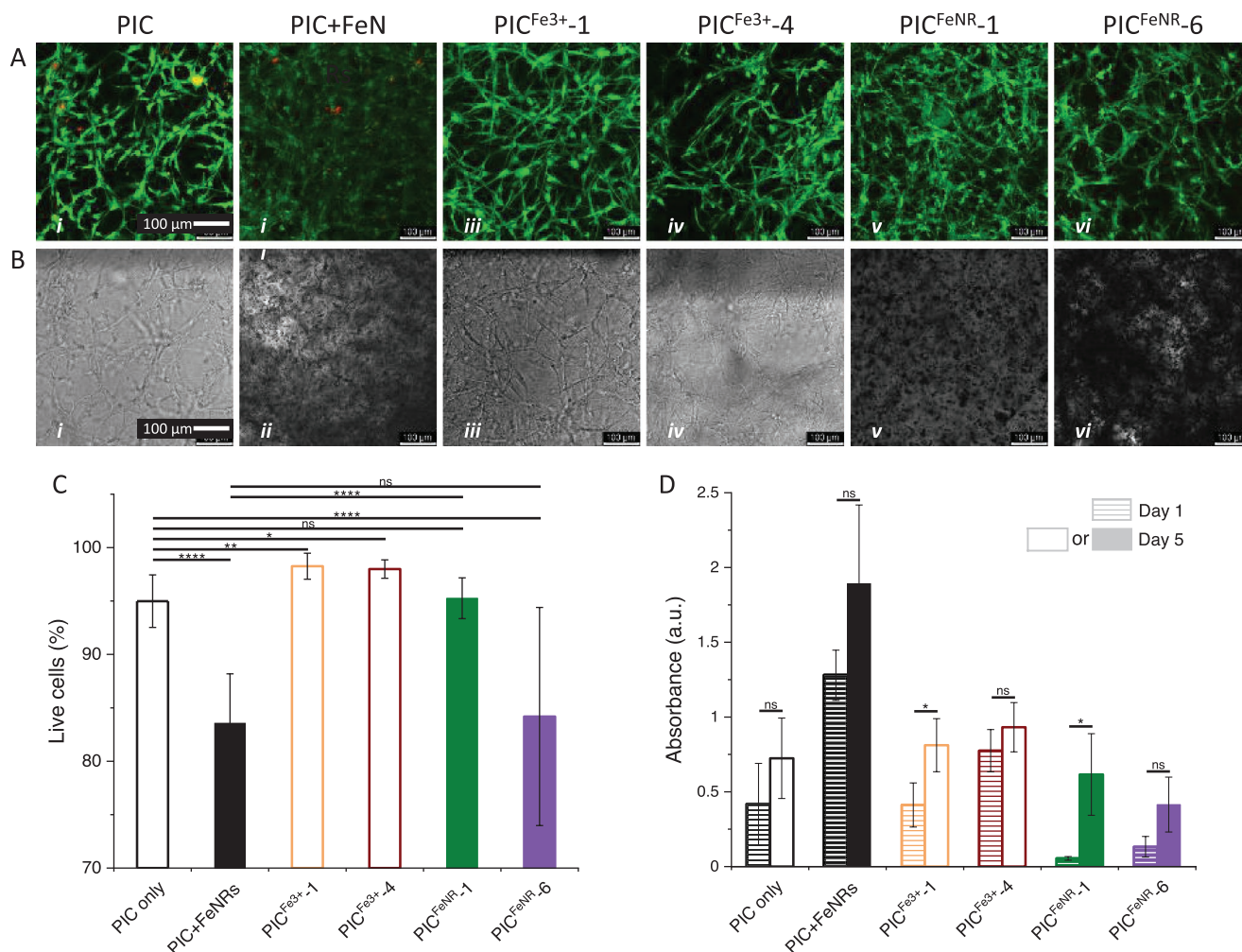


Figure 5. Biocompatibility of the hydrogels. A) Confocal fluorescence images of fibroblasts (HFFs) encapsulated in PIC gels and composites at day 5 after seeding. Living cells (green) and dead cells (red) stained with calcein-AM and TOTO-3, respectively. B) Bright-field images of fibroblasts encapsulated in the different hydrogel groups at day 5 after seeding, showing good strong cell spreading in 3D. Scale bars in (A/B): 100 μm . C) Quantitative analysis of confocal images of living cells (green) and dead cells (red). Data are presented as percentage of live cells, $n = 29$; significance was determined through a one-way ANOVA. D) CCK8 assay results for cell viability at day 1 (striped columns) and day 5 (solid columns); Statistics $n = 3$; Student t -test; p -values > 0.05 , are considered not significant (ns); significant differences: *, $p \leq 0.05$. All data represented as mean \pm standard deviation. The color coding in panels (C) and (D) follows that used in Figure 2.

3. Discussion

So far, it proves exquisitely challenging to realize advanced mechanical properties in artificial materials (either synthetic or reconstituted biological materials) that are able to replicate the soft tissues in our bodies. The typical architecture of these networks is fibrillar, which gives rise to stable highly porous networks at low (bio)polymer densities. Reconstituted biopolymer networks, such as collagen and fibrin indeed show such architectures as well as key mechanical characteristics^[7] such as strain stiffening^[2a] and stress relaxation^[42] but the mechanical parameters are difficult to manipulate, let alone to tailor independently. In synthetic mimics, which are very rare, control over the mechanical properties is typically higher but adaptiveness is mostly limited to a temporary stiffening response (based on strain stiffening) upon external cues such as temperature^[11,23] or magnetic fields.^[30] A viable strategy to push the

current boundaries is to combine the gel with different materials. In this work, we combined fibrous strain stiffening materials with responsive cross-linkers.

The nonlinear stiffening regime of (semiflexible) fibrous hydrogels is characterized by a steep increase in the modulus beyond a critical stress or strain that has been reached in the material. Although the number of hydrogels that display strain stiffening behavior is rapidly increasing,^[10–14] the effect is still not common in synthetic materials. In the literature, two models, an enthalpic and an entropic model are used to describe the effect,^[34] the contribution of each model in a particular network primarily depends on the bending constant of the fibers, which often strongly correlates to their diameter and the density of constituting polymer chains. As such, in situ manipulation of the fibrous architecture through cross-linking is an excellent strategy to manipulate the nonlinear mechanical properties of the hydrogel. Indeed, we observed that the strain

stiffening properties strongly correlate to the concentration of a cross-linker, but only when the cross-linker binds the fibrils. When the cross-linker is embedded in the fibrils, we see no effect on the linear or nonlinear mechanical properties at all.

We emphasize that for the FeNP-cross-linked hydrogels, the mechanical properties are no longer determined by the concentration of polymer or cross-linker, but rather by the connectivity or the density of interactions between the two. In other words, the composition of the mixture does not need to change considerably to change mechanical properties in situ. By using a responsive cross-linker, or in our case, a pH-responsive linkage between the polymer and the cross-linker, one is able to change the interaction density and with that the mechanical properties. Here, we used straightforward magnetic iron oxide nanorods to develop magnetic hydrogels but without stretching the imagination too much, one can think of a variety of functions that such nanoparticle can carry to bring more advanced properties into the material.

The superior properties of the nanoparticle-cross-linked composites compared to the corresponding single component gels are showcased in the self-healing experiments. Although two examples of self-healing and strain stiffening hydrogels have appeared in the literature,^[16,21a] we are unaware of examples of fibrous networks with this combination of properties. A potential reason why they were not found before, for instance, in collagen that simply breaks at high deformations may be explained by the cross-linking mode: only cross-links at the fibril level give effective self-healing properties. Commonly used, small molecule cross-links, like the ferric ions in this paper or other covalent or noncovalent cross-linkers^[29,43] simply bind individual polymer chains, which can be restored after large deformations but do not return an intact branched network.

4. Conclusion

We have prepared a synthetic, highly biomimetic fibrous hydrogel composite with highly adaptive linear and nonlinear mechanical properties. Unlike other materials where the mechanical parameters, particularly the strain stiffening parameters, are typically tailored by the concentration of polymer or cross-linker, in these materials, they are dominated by the connectivity between the polymer and nanoparticles, either through the linker density or the interaction strength between the two components. For the FeNP-cross-linked composites, this results in an approximately fivefold change in stiffness between pH 5 and 9, which is easily realized in situ. We reiterate that the key design principle is the use of a large, multifunctional noncovalent cross-linker, and we believe that this principle may be important for the design of future generation responsive (magnetic, conductive, and light) and adaptive materials.

Recently, PIC hydrogels have been developed as a highly tunable in vitro 3D cell culture matrix^[24b–d,44] with excellent cell biocompatibility. This work presents another strategy to dynamically manipulate the gel's mechanics through nanoparticle cross-linking. At these concentrations, the presence of the nanoparticles in the matrix does not compromise the biocompatibility at the time scale of a week. We foresee that such

dynamic, reversible strategies allow researchers to simply tune “up” or “down” of the mechanical properties of their matrices at will, allowing them to study or drive physiological processes of their in vitro cell cultures, including organoid development or (complex) tissue formation.^[30]

5. Experimental Section

Materials: Details of material preparation are given in the Supporting Information. The linker was synthesized by the reaction between a DBCO and *N*-hydroxysuccinimide (NHS) ester-functionalized spacer and dopamine, as detailed in the Supporting Information. The FeNRs were synthesized following previous reported methods.^[45] The dimensions were analyzed by transmission electron microscopy experiments (Figure S1B–D, Supporting Information): diameter $d \approx 48$ nm, length $L \approx 420$ nm. FeNRs were functionalized with linkers, and the grafting density of linkers on the FeNRs surface was controlled by the concentration of linkers added in the FeNR functionalization protocol and analyzed by a UV–vis spectroscopy protocol (details in the Supporting Information). Unless specified otherwise, the concentrations of PIC and FeNRs in gel composite samples discussed in the paper were both 1 mg mL^{-1} , which meant that the gels contained 99.8 wt% water.

The azide-functionalized PIC polymers were synthesized based on previous reported procedures^[24a,29] with a minor modification, i.e., the fraction azide monomer for the functionalized PIC was increased to 10 mol% in the polymerization reaction. The total monomer to catalyst ratio was 1000:1. Based on viscometry measurements,^[46] the molecular weight of azide-functionalized PIC was $M_w = 358 \text{ kg mol}^{-1}$. For study of mechanical properties, azide–polymers were dissolved in deionized (MilliQ) water. PIC biofunctionalization followed earlier procedures with a minor modification.^[24e] Briefly, a DBCO–GRGDS conjugate was synthesized by the GRGDS peptide (H–Gly–Arg–Gly–Asp–Ser–OH, Bachem Germany) and a DBCO–tetra(ethylene glycol)–NHS (DBCO–PEG4–NHS, Bioconjugate Technologies, Scottsdale) spacer, followed by addition to an (10 mol%) azide-functionalized PIC polymer solution with a 3:10 ratio of DBCO to azide. Note, the remaining azide groups were available for ionic or nanoparticle cross-linking. Then, the biofunctionalized PIC (PIC-RGD) pellets were UV sterilized at 254 nm for 10 min and dissolved in sterile phosphate-buffered saline (8 mg mL^{-1}) at 4 °C overnight. The dissolved polymers were aliquoted and stored at –20 °C until cell seeding.

Preparation of Hydrogel Composite Samples: For the ionic-cross-linked gels, a cold PIC solution ($T = 5$ °C) was mixed with a precooled ($T = 5$ °C) aqueous solution of the cross-linker and iron chloride. The mixture was transferred to the rheometer at 5 °C, which was then heated to 37 °C (well above the PIC gelation temperature $T_{\text{gel}} = 18$ °C). For the nanoparticle-cross-linked composites, the precooled ($T = 5$ °C) and sonicated solution of functionalized FeNRs was added to a cold PIC solution ($T = 5$ °C) and transferred to the rheometer. Note that for the pH studies, the PIC stock solutions were prepared in buffer solutions. After the geometry was closed, the mixture was heated to the desired cross-linking temperature (mostly $T = 50$ °C) and kept at this temperature for 10 h before cooling to 5 °C.

Rheology Measurements: The mechanical properties were analyzed on a Discovery HR-2 rheometer (TA Instruments) using a parallel steel plate geometry with a plate diameter of 20 mm and a gap of 500 μm . The samples were loaded into the rheometer at 5 °C and the geometry was closed. For long time experiments, a layer of silica oil was added to seal the gap to prevent sample dehydration. Then, the samples were heated either quickly or with a controlled rate (1 °C min^{-1}) to the desired temperature where they were equilibrated for a short period (≈ 10 min). The mechanical properties in the linear viscoelastic regime were recorded at a strain amplitude $\gamma = 4\%$ and frequency $\omega = 1$ Hz, unless noted otherwise. The nonlinear response of the hydrogels was evaluated by applying frequency sweep (0.1–10 Hz) with a small stress amplitude superposed on a set prestress σ_0 (with $\sigma < 0.1\sigma_0$).

Note that this prestress protocol was rather time-consuming but gave more accurate results than a simple strain sweep.^[33] Each sample was measured at least 2 times to ensure repeatability.

Cell Culture: Fibroblasts derived from human foreskin were cultured in Dulbecco's modified Eagle's medium in the presence of 10% fetal bovine serum and 1% penicillin/streptomycin until 80–90% confluency was reached, as described previously.^[47] For seeding, cells were harvested using trypsin–ethylenediaminetetraacetic acid (EDTA) treatment, followed by resuspension in complete medium after centrifugation. Cells at a final density of 2×10^5 cells mL⁻¹ were mixed with hydrogels at a concentration of 1 mg mL⁻¹ and seeded on microplates and 96 well plates (uncoated, Ibidi GmbH, Martinsried, Germany) with a volume of 10 or 100 μ L, respectively. After seeding, the plates with the cells 3D encapsulated in the hydrogels were incubated at 37 °C, 5% CO₂ for 30–60 min. Medium (50 μ L for microplate and 200 μ L for 96 well plate) was added on top of the hydrogels, and was refreshed every two days. Note that cell seeding, medium addition, and medium refreshment were carried out inside the cell-culture hood, on a hot plate (37 °C) to avoid resolubilization of the (un-cross-linked) PIC gels. Descriptions of the used assays are given in the Supporting Information.

Statistical Analysis: Statistical analyses of the values for all experiments were presented as mean \pm standard deviation. Statistical analysis (Origin Software) was evaluated for >2 data sets using one-way analysis of variance (ANOVA), followed by paired Student's tests or, for 2 data sets, a paired Student's *t*-test. Propability values $p > 0.05$ were considered not significant. For significant differences: * $p < 0.05$, ** $p < 0.01$, *** $p < 0.001$, **** $p < 0.0001$.

Supporting Information

Supporting Information is available from the Wiley Online Library or from the author.

Acknowledgements

The authors acknowledge Dr. Hans Engelkamp for valuable discussions, the Radboud University workshop TechnoCentre. This research was funded by the China Scholarship Council, Grant Number 201706260280 (W.C.) and the Netherlands Ministry of Education, Culture and Science, Gravitation program Grant No. 024.001.035 (P.H.J.K.).

Conflict of Interest

The authors declare no conflict of interest.

Data Availability Statement

The data that support the findings of this study are available from the corresponding author upon reasonable request.

Keywords

adaptive behavior, biomimetic hydrogels, multiresponsiveness, polyisocyanides, self-healing behavior

Received: March 4, 2022

Revised: June 27, 2022

Published online: August 15, 2022

[1] a) S. Choi, Y. j. Choi, M. S. Jang, J. H. Lee, J. H. Jeong, J. Kim, *Adv. Funct. Mater.* **2017**, *27*, 1703826; b) Y. L. Han, P. Ronceray, G. Xu, A. Malandrino, R. D. Kamm, M. Lenz, C. P. Broedersz, M. Guo,

- Proc. Natl. Acad. Sci. USA* **2018**, *115*, 4075; c) S. Natan, Y. Koren, O. Shelah, S. Goren, A. Lesman, *Mol. Biol. Cell* **2020**, *31*, 1474.
- [2] a) C. Storm, J. J. Pastore, F. C. MacKintosh, T. C. Lubensky, P. A. Janmey, *Nature* **2005**, *435*, 191; b) M. Jaspers, M. Dennison, M. F. J. Mabesoone, F. C. MacKintosh, A. E. Rowan, P. H. J. Kouwer, *Nat. Commun.* **2014**, *5*, 5808.
- [3] S. Motte, L. J. Kaufman, *Biopolymers* **2013**, *99*, 35.
- [4] H. Kang, Q. Wen, P. A. Janmey, J. X. Tang, E. Conti, F. C. MacKintosh, *J. Phys. Chem. B* **2009**, *113*, 3799.
- [5] M. L. Gardel, J. H. Shin, F. C. MacKintosh, L. Mahadevan, N. Matsuda, D. A. Weitz, *Science* **2004**, *304*, 1301.
- [6] K. Aalmo, L. Hansen, E. Hough, K. Jynge, J. Krane, C. Little, C. B. Storm, *Biochem. Int.* **1984**, *8*, 27.
- [7] A. S. G. van Oosten, X. Chen, L. Chin, K. Cruz, A. E. Patteson, K. Pogoda, V. B. Shenoy, P. A. Janmey, *Nature* **2019**, *573*, 96.
- [8] a) A. G. Clark, A. Maitra, C. Jacques, C. Pérez-González, A. Simon, L. Lederer, A. Diz-Muñoz, X. Trepast, R. Voituriez, D. M. Vignjevic, *Nat. Mater.* **2022**, <https://doi.org/10.1038/s41563-022-01259-5>; b) S. Goren, Y. Koren, X. Xu, A. Lesman, *Biophys. J.* **2020**, *118*, 1152.
- [9] A. M. Rosales, K. S. Anseth, *Nat. Rev. Mater.* **2016**, *1*, 15012.
- [10] P. H. J. Kouwer, M. Koepf, V. A. Le Sage, M. Jaspers, A. M. van Buul, Z. H. Eksteen-Akeroyd, T. Woltinge, E. Schwartz, H. J. Kitto, R. Hoogenboom, S. J. Picken, R. J. Nolte, E. Mendes, A. E. Rowan, *Nature* **2013**, *493*, 651.
- [11] M. Fernandez-Castano Romera, R. P. M. Lafleur, C. Guibert, I. K. Voets, C. Storm, R. P. Sijbesma, *Angew. Chem., Int. Ed.* **2017**, *56*, 8771.
- [12] Y. Wang, Z. Xu, M. Lovrak, V. A. A. le Sage, K. Zhang, X. Guo, R. Eelkema, E. Mendes, J. H. van Esch, *Angew. Chem., Int. Ed.* **2020**, *59*, 4830.
- [13] a) K. Bertula, L. Martikainen, P. Munne, S. Hietala, J. Klefström, O. Ikkala, Nonappa, *ACS Macro Lett.* **2019**, *8*, 670; b) J. R. McKee, E. A. Appel, J. Seitsonen, E. Kontturi, O. A. Scherman, O. Ikkala, *Adv. Funct. Mater.* **2014**, *24*, 2706; c) W. Wang, L. Xiang, D. Diaz-Dussan, J. Zhang, W. Yang, L. Gong, J. Chen, R. Narain, H. Zeng, *Chem. Mater.* **2020**, *32*, 10545; d) B. Yan, J. Huang, L. Han, L. Gong, L. Li, J. N. Israelachvili, H. Zeng, *ACS Nano* **2017**, *11*, 11074.
- [14] J. Luo, S. Li, J. Xu, M. Chai, L. Gao, C. Yang, X. Shi, *Adv. Funct. Mater.* **2021**, *31*, 2104139.
- [15] a) L. Han, X. Lu, M. Wang, D. Gan, W. Deng, K. Wang, L. Fang, K. Liu, C. W. Chan, Y. Tang, *Small* **2017**, *13*, 1601916; b) K. Haraguchi, T. Takehisa, *Adv. Mater.* **2002**, *14*, 1120; c) C.-H. Lu, C.-H. Yu, Y.-C. Yeh, *Acta Biomater.* **2021**, *130*, 66.
- [16] D. Mozdehi, S. Ayala, O. R. Cromwell, Z. Guan, *J. Am. Chem. Soc.* **2014**, *136*, 16128.
- [17] Q. Fan, G. Wang, D. Tian, A. Ma, W. Wang, L. Bai, H. Chen, L. Yang, H. Yang, D. Wei, *React. Funct. Polym.* **2021**, *165*, 104963.
- [18] Y. Zhang, B. Yang, X. Zhang, L. Xu, L. Tao, S. Li, Y. Wei, *Chem. Commun.* **2012**, *48*, 9305.
- [19] H. Lee, S. M. Dellatore, W. M. Miller, P. B. Messersmith, *Science* **2007**, *318*, 426.
- [20] L. Li, B. Yan, J. Yang, L. Chen, H. Zeng, *Adv. Mater.* **2015**, *27*, 1294.
- [21] a) M. Krogsgaard, M. A. Behrens, J. S. Pedersen, H. Birkedal, *Biomacromolecules* **2013**, *14*, 297; b) S. Azevedo, A. M. Costa, A. Andersen, I. S. Choi, H. Birkedal, J. F. Mano, *Adv. Mater.* **2017**, *29*, 1700759.
- [22] J. Sedó, J. Saiz-Poseu, F. Busqué, D. Ruiz-Molina, *Adv. Mater.* **2013**, *25*, 653.
- [23] P. de Almeida, M. Jaspers, S. Vaessen, O. Tagit, G. Portale, A. E. Rowan, P. H. J. Kouwer, *Nat. Commun.* **2019**, *10*, 609.
- [24] a) R. K. Das, V. Gocheva, R. Hammink, O. F. Zouani, A. E. Rowan, E. Oosterwijk, P. H. Kouwer, *Biomacromolecules* **2019**, *20*, 826; c) S. Ye, J. W. B. Boeter, M. Mihajlovic, F. G. van Steenbeek, M. E. van Wolferen, L. A. Oosterhoff, A. Marsee, M. Caiazzo,

- L. J. W. van der Laan, L. C. Penning, T. Vermonden, B. Spee, K. Schneeberger, *Adv. Funct. Mater.* **2020**, *30*, 2000893; d) Y. Zhang, C. Tang, P. N. Span, A. E. Rowan, T. W. Aalders, J. A. Schalken, G. J. Adema, P. H. J. Kouwer, M. M. P. Zegers, M. Ansems, *Adv. Sci.* **2020**, *7*, 2001797; e) J. Kumari, F. A. D. T. G. Wagener, P. H. J. Kouwer, *ACS Appl. Mater. Interfaces* **2022**, *14*, 19212.
- [25] R. C. op 't Veld, O. I. van den Boomen, D. M. S. Lundvig, E. M. Bronkhorst, P. H. J. Kouwer, J. A. Jansen, E. Middelkoop, J. W. Von den Hoff, A. E. Rowan, F. A. D. T. G. Wagener, *Biomaterials* **2018**, *181*, 392.
- [26] a) B. Wang, J. Wang, J. Shao, P. H. J. Kouwer, E. M. Bronkhorst, J. A. Jansen, X. F. Walboomers, F. Yang, *J. Controlled Release* **2020**, *324*, 134; b) B. Wang, H. E. Booi-Vrieling, E. M. Bronkhorst, J. Shao, P. H. J. Kouwer, J. A. Jansen, X. F. Walboomers, F. Yang, *Acta Biomater.* **2020**, *116*, 259.
- [27] L. Gerrits, R. Hammink, P. H. J. Kouwer, *Polym. Chem.* **2021**, *12*, 1362.
- [28] a) M. Jaspers, A. E. Rowan, P. H. J. Kouwer, *Adv. Funct. Mater.* **2015**, *25*, 6503; b) P. de Almeida, P. A. Janmey, P. H. J. Kouwer, *Adv. Funct. Mater.* **2021**, *31*, 2010527.
- [29] D. C. Schoenmakers, A. E. Rowan, P. H. J. Kouwer, *Nat. Commun.* **2018**, *9*, 2172.
- [30] W. Chen, Y. Zhang, J. Kumari, H. Engelkamp, P. H. J. Kouwer, *Nano Lett.* **2021**, *21*, 6740.
- [31] W. Chen, P. H. J. Kouwer, *Adv. Funct. Mater.* **2021**, *31*, 2105713.
- [32] Note that cross-linking for both composites proceeds above the gelation temperature; here, the fibrous network is formed that accelerates the cross-linking reaction.
- [33] C. P. Broedersz, K. E. Kasza, L. M. Jawerth, S. Munster, D. A. Weitz, F. C. MacKintosh, *Soft Matter* **2010**, *6*, 4120.
- [34] C. P. Broedersz, F. C. MacKintosh, *Rev. Mod. Phys.* **2014**, *86*, 995.
- [35] D. A. Head, A. J. Levine, F. C. MacKintosh, *Phys. Rev. Lett.* **2003**, *91*, 4.
- [36] a) P. R. Onck, T. Koeman, T. van Dillen, E. van der Giessen, *Phys. Rev. Lett.* **2005**, *95*, 178102; b) M. Fernández-Castaño, Romera, X. Lou, J. Schill, G. ter Huurne, P.-P. K. H. Fransen, I. K. Voets, C. Storm, R. P. Sijbesma, *J. Am. Chem. Soc.* **2018**, *140*, 17547.
- [37] a) F. Huber, A. Boire, M. P. López, G. H. Koenderink, *Curr. Opin. Cell Biol.* **2015**, *32*, 39; b) L. Blanchoin, R. Boujemaa-Paterski, C. Sykes, J. Plastino, *Physiol. Rev.* **2014**, *94*, 235.
- [38] a) B. P. Lee, S. Konst, *Adv. Mater.* **2014**, *26*, 3415; b) M. J. Harrington, A. Masic, N. Holten-Andersen, J. H. Waite, P. Fratzl, *Science* **2010**, *328*, 216.
- [39] For the pH experiments, potassium phosphate buffer solutions were used rather than MilliQ (see the Experimental Section).
- [40] a) K. M. Wisdom, K. Adebowale, J. Chang, J. Y. Lee, S. Nam, R. Desai, N. S. Rossen, M. Rafat, R. B. West, L. Hodgson, O. Chaudhuri, *Nat. Commun.* **2018**, *9*, 4144; b) K. Liu, M. Wiendels, H. Yuan, C. Ruan, P. H. Kouwer, *Bioact. Mater.* **2021**, *9*, 316.
- [41] P. AshaRani, G. Low Kah Mun, M. P. Hande, S. Valiyaveetil, *ACS Nano* **2009**, *3*, 279.
- [42] O. Chaudhuri, J. Cooper-White, P. A. Janmey, D. J. Mooney, V. B. Shenoy, *Nature* **2020**, *584*, 535.
- [43] S. R. Deshpande, R. Hammink, R. K. Das, F. H. T. Nelissen, K. G. Blank, A. E. Rowan, H. A. Heus, *Adv. Funct. Mater.* **2016**, *26*, 9075.
- [44] a) Z. Zhang, W. Chen, D. M. Tiemessen, E. Oosterwijk, P. H. J. Kouwer, *Adv. Healthcare Mater.* **2022**, *11*, 2102389; b) B. M. Tiemeijer, M. W. D. Sweep, J. J. F. Sleeboom, K. J. Steps, J. F. van Sprang, P. De Almeida, R. Hammink, P. H. J. Kouwer, A. I. P. M. Smits, J. Tel, *Front. Bioeng. Biotechnol.* **2021**, *9*, 715408.
- [45] W. Xu, M. Wang, Z. Li, X. Wang, Y. Wang, M. Xing, Y. Yin, *Nano Lett.* **2017**, *17*, 2713.
- [46] M. Koepf, H. J. Kitto, E. Schwartz, P. H. J. Kouwer, R. J. M. Nolte, A. E. Rowan, *Eur. Polym. J.* **2013**, *49*, 1510.
- [47] D. M. Lundvig, S. W. Pennings, K. M. Brouwer, M. Mtaya-Mlangwa, E. A. Mugonzibwa, A. M. Kuijpers-Jagtman, J. W. Von den Hoff, F. A. Wagener, *Exp. Cell Res.* **2015**, *330*, 429.